Debye screening in the QCD gluonic plasma

Mingshen Gao
Advanced Computer Program, Fermi National Laboratory, P.O. Box 500, Batavia, Illinois 60510
(Received 1 May 1989; revised manuscript received 14 September 1989)

Studies on the static screening effect in a pure gluon plasma by an extensive numerical simulation of lattice QCD is reported here. The simulation is done on a $24\times24\times24\times N_t$ lattice with $N_t=4,6,16$ at various temperatures above the phase transition. Our results show that the hot gluon plasma fits a Debye-screening picture very well and the potential for each representation of a $q\bar{q}$ pair system is of Yukawa-type potential. Also, accidentally, we find that the potential tends to agree with the naive "lowest-order perturbative prediction" when T becomes much larger than T_c.
MS code no. DE4109 1990 PACS number(s): 12.38.Mh, 11.15.Ha, 12.38.Gc

I. INTRODUCTION

The nature of the quark and gluon plasma in the deconfined phase is not understood yet. It is expected from asymptotic freedom that the quark and gluon plasma may be described approximately as a gas of weakly interacting quarks and gluons, at least for high temperatures. In analogy to a QED hot plasma, where the Debye-screening picture gives a good description of its dynamic properties, we expect that a similar picture will also be suitable for the QCD plasma. However, from the theoretical point of view, the justification for this is hard to make because of the great difficulties in dealing with the infrared divergences in finite-temperature perturbative QCD even at extremely high temperatures. Nonperturbative qualitative results are necessary.

Debye screening refers to the long-distance shielding of electric charge (or color charge here) by plasma excitations and converts the Coulomb potential into a Yukawa potential. A further quantitative understanding of the screening effect is very important since it might be the physical mechanism responsible for the color deconfinement phase transition.[1] The low-energy elementary excitations of the hot plasma can also be learned from this study since it is related indirectly to the screening effect.[2] In addition, the heavy-quark potential in such a phase can provide valuable information for high-energy heavy-ion collisions. These are also motivations for this study.

In this paper, we will report our high-statistics Monte Carlo simulation result for quark and gluon plasma. Our simulation results on lattice QCD clearly support the Debye picture. Based on it, we made a good measurement of the static heavy-quark potential between q and $\bar{q}$ and the "Debye" mass of the gluon plasma.

This paper is organized as follows. In Sec. II we discuss the T dependence of the static heavy-quark potential based on the Debye picture and the perturbative results. In Sec. III we discuss the computation and fit of the Wilson line correlations (WLC). In Sec. IV we present and discuss our simulation results. And finally, in Sec. V, we give the conclusions.

II. HEAVY-QUARK POTENTIAL FROM A DEBYE SCREENING PICTURE

At low temperature, the QCD [SU(3) gauge field theory] system is confined. Quarks are found to live only inside the hadronic matter. Thus, they are not part of the (low-energy) eigenstates of the QCD Hamiltonian but their bound states are. Heating of the QCD system causes a deconfinement phase transition. The free energy of an isolated quark changes from infinite to finite as a result of the phase transition. After the phase transition, quarks are released from their bound states so that the basic components (low-lying energy eigenstates) for the QCD system becomes the quarks and gluons which form the interacting plasma; this is the QCD plasma. In this paper, we will concentrate on one of its static properties, the static heavy-quark potential which relates to the dynamics of the hot QCD system directly. We have made the study through large-volume and high-statistics Monte Carlo simulation. Previous works in this field can be found in Ref. 3.

The starting point for our study is the correlation function between thermal Wilson lines. The correlation function for two Wilson lines separated by an arbitrary spatial displacement $\mathbf{R}=(x,y,z)$ is defined as (on the lattice)

$$\Gamma(\mathbf{R})=\left\langle \sum_{\mathbf{x}} \frac{1}{N_s^3}[L(\mathbf{x})L^{\dagger}(\mathbf{x}+\mathbf{R})] \right\rangle , \tag{1}$$

where

$$L(\mathbf{x})=\tfrac{1}{3}\mathrm{Tr}\left[\prod_{t=1}^{N_t} U_{\mathbf{x};t,t+1} \right] . \tag{2}$$

Since the averaged value of $L(\mathbf{X})$ is related to the free energy $\mathcal{F}_q$ of an isolated static heavy quark by $L=\langle (1/N_s^3)\sum_{\mathbf{x}} L(\mathbf{x})\rangle \sim \exp(-\mathcal{F}_q/T)$, we expect that the free energy for a static $q\bar{q}$ pair relates to Γ by

$$\begin{aligned}\Gamma(\mathbf{R}) &\sim \exp[-(F_{q\bar{q}}+\mathcal{F}_q+\mathcal{F}_{\bar{q}})/T] \\ &\sim LL^{\dagger}\exp[-V(T,\mathbf{R})/T] .\end{aligned} \tag{3}$$

The free energy of a static $q\bar{q}$ system is the interacting po-

tential $V_{q\bar{q}}$ which is related to the dynamics of a $q\bar{q}$ pair system. By measuring $[\Gamma(\mathbf{R})]$, we can get a qualitative measurement on $V(T,\mathbf{R})$. This provides us with valuable information on the dynamic properties of a $q\bar{q}$ system as well as more information about the nature of the mechanism of the phase transition.

Based on an analogy to the hot QED plasma, we expect that the dynamics of the QCD plasma also fit the Debye picture even though this system may actually interact very strongly and the analogy might be very loose. The Debye picture provides us with

$$V(T,\mathbf{R})=\mathcal{C}(T)\exp[-m_D(T)|\mathbf{R}|]/|\mathbf{R}| , \tag{4}$$

where m_D is the Debye screening mass which is one of the characteristics of the hot QCD plasma and $\mathcal{C}$ is the coupling strength. However, since a $q\bar{q}$ pair could be in either a singlet or an adjoint (octet) representation at least in the weak-coupling region, there are actually two potentials from the two representations corresponding to the single correlation. Thus, we expect for the correlation (as given by Refs. 3 and 4)

$$\begin{aligned}\Gamma/|L|^2 &\sim \tfrac{1}{9}\mathrm{Tr}(e^{-H_s/T})+\tfrac{8}{9}\mathrm{Tr}(e^{-H_a/T}) \\ &= \tfrac{1}{9}e^{-V_s/T}+\tfrac{8}{9}e^{-V_a/T} .\end{aligned} \tag{5}$$

Qualitative prediction about the asymptotic behavior of Eq. (5) for two special regions could be derived in a simple physical but not mathematically strict way. We need these predictions to guide fitting our Monte Carlo data and our fits will check these predictions. This is the motivation for the following discussion.

Let us consider the $T\gg T_c$ case first. When $T\gg T_c$, where we may assume asymptotic freedom so that perturbation theory might be a reasonable approximation.[5] Then we could borrow some of the perturbative results to give a naive "perturbative potential." The lowest-order perturbative result (on an infinite lattice or in the continuum limit) gives $\mathcal{C}_{s,a}=(g^2/4\pi)F_{s,a}$, where $F_{s,a}=-\frac{4}{3},\frac{1}{6}$ are factors from group theory so that $\frac{1}{9}\mathcal{C}_s+\frac{8}{9}\mathcal{C}_a=0$. Also, the resummation of electric mass gives us $m_D=m_E\sim gT$, where m_E is the electric mass. If these results could be applied, and let us assume that both V_s and V_a are given by Eq. (4) as $V_{s,a}\sim\mathcal{C}_{s,a}e^{-m_DR}/R$, then the connected part of Γ at larger R will be given by

$$\Gamma(\mathbf{R})/|L|^2-1\sim\mathcal{C}e^{-2m_ER}/R^2 , \tag{6}$$

since the $1/R$ leading term has been canceled out among the two possible representations where $\mathcal{C}\sim\frac{1}{18}C_s^2+\frac{4}{9}\mathcal{C}_a^2\sim(1/9T^2)(g^2/4\pi)^2$.

Strictly speaking, whether or not the lowest-order perturbative results could be trusted is not clear yet because of the severe divergence of higher orders which is not understood yet (further discussion can be found from Refs. 4 and 5). But this does lead us to a possible asymptotic potential for $T\gg T_c$,

$$V(R,T)=\mathcal{C}(T)\frac{\exp[-\mu(T)R]}{(RT)^2} , \tag{7}$$

where $\mu(T)\sim 2gT$. It turns out that our large-volume high-statistics simulation result agree with this naive potential, a blinded "lowest-order perturbative result," very well.

When T is not too much higher than T_c, high-order terms (more complicated processes with multiple gluon exchanges) of a possibly nonperturbative character become more important. Even though we may still assume the Debye-type potential for each representation, but the T dependence of m_D and $\mathcal{C}$'s might become more complicated. Such, in contrast with $T\gg T_c$ region where the effective "single massive gluon exchange" process is dominant for each representation which leads to the cancellation of $1/R$ term, there is no more cancellation in the leading $1/R$ term so that

$$\Gamma(\mathbf{R})/|L|^2-1\sim\mathcal{C}e^{-m_DR}/R , \tag{8}$$

where $\mathcal{C}\sim\frac{1}{9}\mathcal{C}_s+\frac{8}{9}\mathcal{C}_a$. In fact, as $T\to T_c^+$, the interaction becomes much stronger. It is possible for a bare quark to be easily covered by gluons to form more complicated color states. Then its influence to the other quark becomes less and less dependent on the representation. It is known that the leading part of the confined potential has nothing to do with whichever representation it belongs to. Influenced by this confining character, it is expected that the potentials corresponding to the two representations become less and less distinguishable. As a result, there will only be a single exponential term with $\Gamma\sim\exp(\mathcal{C}e^{-\mu r}/r)$ instead of Eq. (5) for $T\sim T_c^+$. Now, the asymptotic potential becomes

$$V(R,T)=\mathcal{C}(T)\frac{\exp[-\mu(T)R]}{RT} . \tag{9}$$

The above two distinctive regions [$n=1$ and $n=2$ for $V(r)\sim e^{-\mu r}/r^n$] are the most interesting regions and their existence is verified by our simulation (Sec. III). This is one of the major results of this calculation. Also it is found that a transition region exists in between where there is strong competition in the $1/R$ term and $1/R^2$ term. It is interesting to notice that, although the perturbative results suffer an unexpected breakdown even at the next order (Ref. 4) and finite-temperature QCD perturbative theory also suffers infrared divergence beginning at $O(g^6)$ even at very high temperature, which throws a shadow on the entire idea of perturbatively computing the Debye mass,[4] our naive prediction does predict our lattice QCD simulations. The WLC data are well behaved and well measured in the lattice. By fitting them to an expected theoretical function forms such as Eqs. (5), (6), and (8), we can get a good measurement of the parameters such as the $\mathcal{C}$'s and μ including their T dependence. [Since it is more convenient to use $\mu(T)$ than m_D or $2m_D$, we will define μ as the screening mass for the whole temperature range for the rest of the paper.] This is the subject of the next few sections.

III. WILSON LINES CORRELATION

Our simulation started with the computation of the correlation function for two Wilson lines defined in the previous section. The correlation function $[\Gamma(\mathbf{R})]$ can be well measured from Monte Carlo simulations. In this

section we will discuss the measurement and fitting of (Γ). In Sec. IV we discuss the results.

In a typical Monte Carlo simulation of lattice QCD, most of the time is spent in generating the configurations. This is the dominant computation. In order to use the data effectively and save CPU time, we have calculated $\Gamma(\mathbf{R})$ for all the possible $\mathbf{R}$'s. Traditionally, (Γ) is only measured on the axes because of the difficulties discussed later. There are several obvious advantages for measuring the whole (Γ); first, the angular dependence and the restoration of the rotational symmetry can be studied; second, a fitting range enlarged by a factor of $\sqrt{3}$ can be accessed such that we can get long-range asymptotic behavior beyond the $N_s/2$ limit; third, more points in the fitting reduces the errors and helps to determine which functional form is the best or right one.

However, the calculation of all the possible correlation $[\Gamma(\mathbf{R})]$ is more complicated. The number of operations for calculating one set of (Γ) is about $\sim 8N_s^6$, which is $\sim 10^9$ for our $N_s=24$ case. The memory requirement is about half a mega for storing a single set of (Γ). These are large numbers for a serial-architecture single CPU computer such as a VAX. The program needs about 30 min of CPU time to calculate a single set of (Γ) on a VAX/780. Since the problem is homogeneous with apparent, intrinsic parallelism, it is suitable for parallel-processor systems. Here, the difficulty is that the data are possibly distributed over all the local memories associated with different processors and the communication overhead among multiple processors potentially degrades the efficiency.

My program is written for the 64-node parallel supercomputer designed and built at Columbia University.[6,7] It is a dedicated parallel processor system for lattice QCD simulations. By creating communication buffers on each processor, taking advantage of its two-dimensional lattice architecture and playing tricks with the data communication,[8,9] the overhead can be eliminated. The execution time is about 2 sec. This shows how fast our machine can be compared to 30 min on the VAX.

The configurations are generated by a mixture of a Cabibbo-Marinari pseudo-heat-bath algorithm and a microcanonical algorithm. The number of sweeps for each run is determined by N_t and β. Typically, we run 50 000 to 150 000 sweeps for $N_t=16$ case and 10 000 to 150 000 for $N_t=4,6$. The WLC is measured every two sweeps. After dropping the nonequilibrium part for each dedicated run associated with some $\{N_t,\beta\}$, we either average the data over all sweeps to get the set of $[\Gamma(\mathbf{R})]$ and fit it to an expected functional form to get the best-fit parameters, or we use the jackknife method to get errors for the fitted parameters by separating the data of different sweeps into a number of pieces (5–10 typically).

Because of the cubic symmetry and the topology of the lattice, the number of independent $[\Gamma(\mathbf{R})]$ can be greatly reduced. We can average over the reflection of axes first, this reduces the number of correlations from 24^3 ($N_s=24$ in our case) to 2197 independent Γ's. Then we average and sort them further to $[\Gamma(d_1,d_2,d_3):0\le d_1\le d_2\le d_3\le N_s/2]$ according to the permutation or rotation of (x,y,z) before we start the fitting. Only 454 correlations are left, but all information such as the angular dependence is still contained in them.

Since the lattice is a three-dimensional torus, a color charge interacts with another charge in such a way that the charge itself and seven of its images formed by the periodic boundaries contribute simultaneously. We have to modify the fitting functions to take care of the effect of all these images. We can denote the separations between them and the test charge by $R_i=|\mathbf{R}-\mathbf{R}_{bc}|$, $i=1,\ldots,8$ with $\mathbf{R}_{bc}=(0,0,0),(N_s,0,0),(N_s,N_s,0),(N_s,N_s,N_s)$ and their permutations. We will see their influence later.

Our fitted parameters are obtained from the least-square fits of expected theoretical functions with the $[\Gamma(d_1,d_2,d_3)]$ mentioned above. Figure 1 shows a typical fit. It is for $\beta=8.00h$ (h means a hot start) on a $24^3\times 6$ lattice. We will limit the fitting range to be $R_1\in[R_{\min},R_{\max}]$, where R_1 is the smallest of the radii $\{R_i:i=1,\ldots,8\}$. Since a set of (d_1,d_2,d_3) will uniquely determine $\{R_i:i=1,\ldots,8\}$, we actually sum over all the possible $\{d_i:i=1,2,3\}$ within $[R_{\min},R_{\max}]$.

Two criteria should be proposed before we discuss our fitted results. The fitted results are considered as good results only when the following two criteria are satisfied: χ^2 should be small and the best-fitted parameters should not be influenced by different selections of $[R_{\min},R_{\max}]$. The first one is evident since it is the quality of the fits. The second one is also very important since it reflects the correctness of the fitting function. If the fitting function is the right function, then it should not be sensitive to which part of the data is used to fit the parameters. Of course, if it is not the right one, different parts of the data will give different parameters. The systematic dependence on $R_{\min}$ or $R_{\max}$ can be used to select the better function, this is the bottom line for the second criterion.

IV. SIMULATION RESULTS

A. Results for lattice of size $24^3\times 16$

We have made extensive simulations here, which is so far the largest lattice encountered. We have obtained almost 100 000 sweeps for each one of the points at $\beta=6.6,6.7,6.8$ ($\beta_c\sim 6.5$). Since the onset of scaling begins at about $N_t=10$ and $\beta=6.0$, these points are expected to be very close to the continuum limit.

These points clearly belong to the deconfined phase and are close to the transition point. So we get a good chance to study the dynamic properties of hot QCD plasma right above the transition point, which should be the most interesting region for heavy-ion-collision experiments.

As discussed previously, the toroidal boundary condition forms eight effective charges (charge itself and seven of its images). In real fitting, the fitting function has to be modified to include the effect. In the deconfined phase, since the force field is a three-dimensional one so that all eight charges formed by the periodic boundaries can feel the existence of a color charge and contribute to the interacting potential simultaneously. Then,

$$\Gamma(\mathbf{R})=|LL^{\dagger}|\exp\left[\sum_{i=1}^{8}-V(\mathbf{R}_i,T)/T\right], \tag{10}$$

becomes the real fitting function. In the rest of this paper, all the fitting we are talking about is actually done based on this equation with some proper potential $V(\mathbf{R},T)$. For example, Fig. 1 shows a typical fit of Eq. (10) with a potential $\mathcal{C}\exp(-\mu R)/R^2$. The measured data fit the above expectation very well.

First, let us see how can we use the second criterion to select the right fitting function. As discussed in the first section, the systematic dependence on the selections of $[R_{\min},R_{\max}]$ can be used to select the right function. The following is a good example. It is demonstrated in Fig. 2. The lattice size used is $24^3\times 16$ and the β is $6.80h$. If we fit (Γ) with a simple exponential decay function

$$\Gamma(\mathbf{R})\sim A+B\sum_{i=1}^{8}\exp(-\mu R_i), \tag{11}$$

as used by Ref. 2 for the screening mass, we get the fitted screening masses for different selections of $[R_{\min},R_{\max}]$ shown by the crosses in Fig. 2. These result suffer a systematic influence due to the missing $1/R^n$ factor. This is especially true since the simulation is limited to a finite lattice ($R_{\max}<21$ in our case which is one of the largest separations so far found in current simulations). The missing $1/R^n$ factor, (which can be written as $-n\times\log R$ in the exponential and expanded as a linear function since it is relatively flat in the region $[R_{\min},R_{\max}]$), does contribute an extra portion to the screening mass depending mostly on $R_{\min}$. By inserting the right R^n factor (results with $n=1,2$ are shown by circles and stars in the figure)

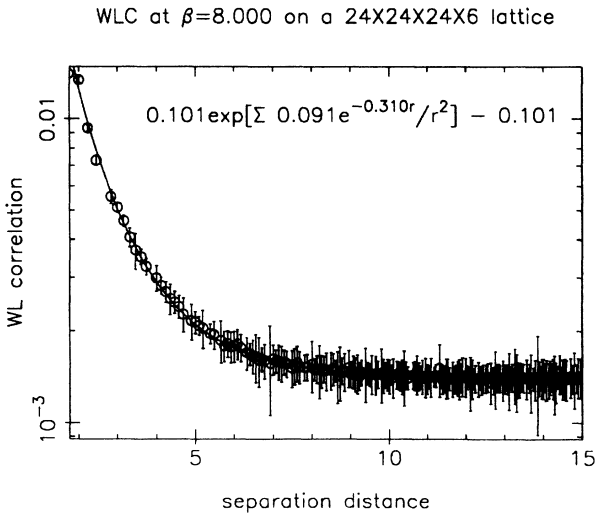

FIG. 1. A typical fitting for WLC. The circles and corresponding error bars are the measured WLC while the curve is simply a direct line segment connection of calculated WLC points from the fitted function. (The evaluation of the fitted function is made on a lattice of exactly the same size.)

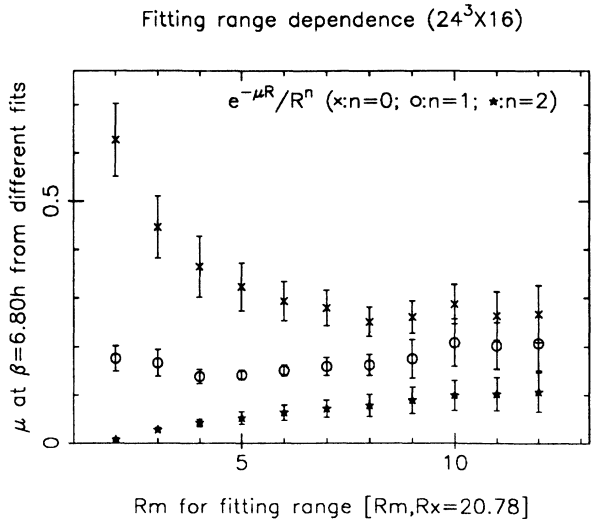

FIG. 2. Fitting-range dependence of the screening mass. More exactly, fitted μ is plotted as a function of $R_{\min}$ which determines the fitting range to be $[R_{\min},12\sqrt{3}]$. For $n=0,1,2$ the corresponding fitting functions at large R are given by Eqs. (11), (9), and (7). In real fits, the function has been modified to include all the eight effective charges.

to the fitting function, the systematic dependence is clearly removed. Figure 2 shows that the choice $n=0$ or 2 has a strong systematic influence on the screening mass while the right choice $n=1$ does not. It is clear that $1/R$ is the right factor and $\exp(-\mu R)/R$ is the right potential in this case, where $T\sim 1.35T_c$.

Similar results are also true for both $\beta=6.6$ and 6.7 cases. Detailed results about the Debye screening mass (inverse of screening length) will be given by Ref. 10. Our conclusion is that the simple Debye potential $\exp(-\mu R)/R$ is the leading static heavy-quark potential for $T_c<T<1.4T_c$. Here, T/T_c is calculated by

$$\frac{T}{T_c}=\left[\frac{g}{g_c}\right]^{102/121}\exp\left[\frac{8\pi^2}{11}\left[\frac{1}{g^2}-\frac{1}{g_c{}^2}\right]\right], \tag{12}$$

where $g=\sqrt{6/\beta}$ and $g_c=\sqrt{6/\beta_c}$.

B. Dynamic properties of the hot QCD at $T\sim T_c$ and $T\gg T_c$ ($N_t=4,6$)

An important discovery from this simulation is that the long-distance asymptotic behavior at large R is different in the regions $T\sim T_c{}^+$ ($T_c<T<1.4T_c$) and $T\gg T_c$ ($T>3.5T_c$), just as expected from our discussion in Sec. II. The comparison for fitting Eq. (10) with $[V(\mathbf{R})=\mathcal{C}e^{-\mu R}/R^n, n=1,2]$ is shown by Figs. 3(a) and 3(b). Here, the simulation is done on the $24^3\times 6$ lattice. While $1/R$ is better for the region where T is close to T_c (roughly, $T<1.4T_c$), $1/R^2$ is better for the region where T is much larger than T_c (roughly $T>3.5T_c$). This is consistent with the expectation of Eqs. (7) and (9). This verifies the existence of the 2 special regions.

In between the two regions, it is more complicated.

Neither Eq. (7) nor (9) gives us a consistent fit. However, it is possible to fit using the complete formula Eq. (5) with two disjoint choices of the parameters: either $-\mathcal{C}_s$ and $8\mathcal{C}_a$ tend to cancel to give $1/R^2$ or both $-\mathcal{C}_s$ and $8\mathcal{C}_a$ deviate from each other to give $1/R$. Both fits are good and strong competition between the two is evident. So, Eq. (5) appears to be the fitting function we expected. But errors are large and the results from the two different choices in parameters cannot be distinguished within 2 standard deviations.

Figure 4 shows our results for $N_t=6$ at various T's. The lowest-order perturbative results at high temperature are also shown by the curve in Fig. 4. A dip associated with the phase transition exists near $T\sim T_c{}^+$. After reaching a maximum at about $T\sim 1.5T_c$ as T increases from $T_c{}^+$, it begins to decrease towards the curve predicted by the perturbative theory. The last two results at $\beta=7.0$ and 8.0 are obtained by fitting with $n=2$ and results for $\beta\leq 6.0$ are obtained with $n=1$. The result for $\beta=6.4$ are obtained by fitting Eq. (5).

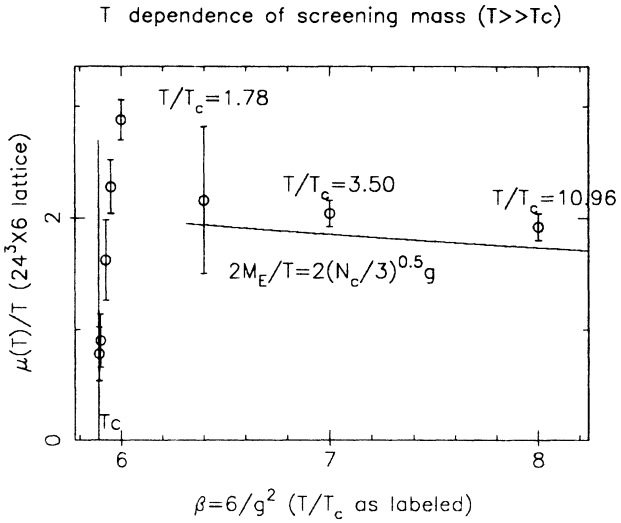

FIG. 4. Screening mass at various temperatures. [$g=\sqrt{6/\beta}$ is related to T/T_c and $\beta_c=6/g_c^2\sim 5.891$ by Eq. (12)]. The measurement is done on a $24^3\times 6$ lattice with T/T_c ranging from 1.0 to 11.0 and $\mu(T)$ is defined by $V(R,T)=\mathcal{C}(T)\{\exp[-\mu(T)R]\}/(RT)^n$ with $n=1,2$ for $T\sim T_c$ and $T\gg T_c$, respectively.

The tendency for agreement of the screening mass at high T with the perturbative predictions ($2m_E$) is clear. Similar conclusions can also be drawn from $\mathcal{C}_s$ and $\mathcal{C}_a$ shown below in Fig. 5. Note, there is a small difference (~ 1.5 standard deviation) between the measured results

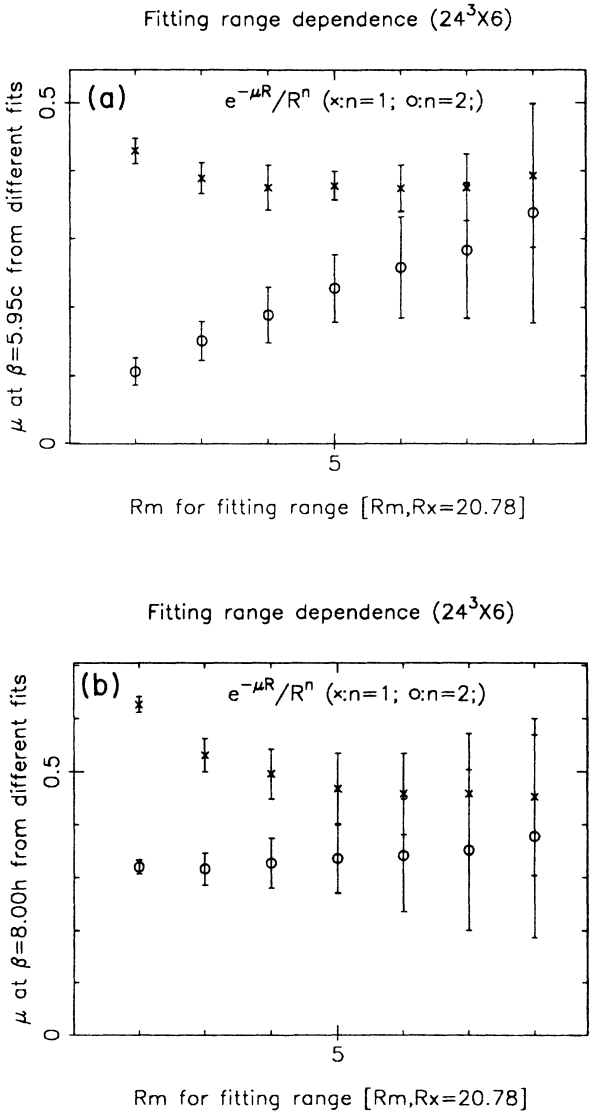

FIG. 3. Comparison with fittings Eqs. (7) and (9) for different temperatures. This is done in analogy with Fig. 2.

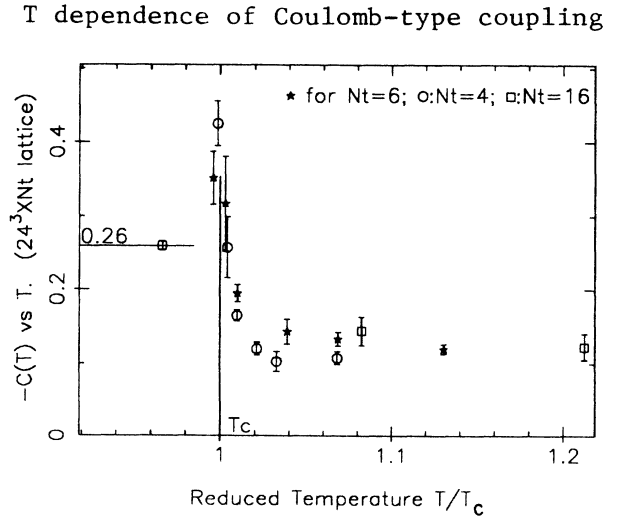

FIG. 5. T dependence of the coupling strength near T_c. The measurement is done on $24^3\times N_t$ lattices with $N_t=4,6,16$ and $\mathcal{C}(T)$ is defined by Eq. (9).

and the curve. If we use $\mu \sim x m_E$, we will get $x \sim 2.2$ instead of $x=2$. The discrepancy might be caused by the finite lattice spacing error due to small N_t or it might be real if it is not caused by the statistics. It would be clear if we could increase N_t. But anyway, it shows that the gauge theory at high temperature meets the expectation of the asymptotic freedom. The onset of the asymptotic region begins at about $3.5T_c$.

Now, let us look at the coupling strength. Near T_c^+, the interaction is very strong so that it does not make a lot of sense to distinguish the two representations as discussed in the previous section. Our correlation fits a single exponential [Eq. (10)] with $V(\mathbf{R})=\mathcal{C}e^{-\mu R}/R$ very well for this region just as expected. Further, by fitting the correlation with Eq. (5), we can easily verify that $\mathcal{C}_s$ and $\mathcal{C}_a$ turn out to be the same even though I have inserted a different sign for V_s and V_a. Also, we have noticed that the coupling $\mathcal{C}$ here seems to be a continuation of the coupling from the Coulomb term in the confined potential.[9] Figure 5 shows $\mathcal{C}(T)$ for $N_t=4,6,16$ and they all have the similar behavior. It also shows the strong N_t dependence. Result from $N_t=4$ is about 60% higher than the result from $N_t=16$ [measured at the point near the critical temperature $T \sim T_c$ in the confined phase since $\mathcal{C}$ is roughly a constant for each N_t (Ref. 9)]. While it decreases much more rapidly for small N_t, it decreases very slowly for large N_t. Part of this is possibly caused by the scaling violation at small N_t since a two-loop perturbative scaling function is used for calculating the reduced temperature T/T_c.

At high T, things become different. Figure 6 shows the results for the T dependence of $\mathcal{C}_{s,a}$ at those T's that are not close to T_c^+. It is clear that $\mathcal{C}_a$ has changed sign and magnitude so that $8\mathcal{C}_a$ tends to agree with $-\mathcal{C}_s$. More important, both $\mathcal{C}_s$ and $\mathcal{C}_a$ shows a clear tendency to agree with the expectation of lowest-order perturbative results $-\frac{4}{3}g^2/4\pi$ and $\frac{1}{6}g^2/4\pi$. (The last two measured points at high T are systematically higher than the curve, roughly about 2 standard deviations. The difference is most likely due to the finite N_t used here since Fig. 5 shows clearly that finite N_t influence $\mathcal{C}$ significantly.)

C. F_q for $N_t=4,6$ near the phase transition

We have obtained very high-statistics results near the critical point at $N_t=4,6$ in order to understand more about the nature of the phase transition better. The WLC in the neighborhood of the phase transition fits

$$\Gamma(\mathbf{R}) \sim |L|^2 \exp\left[\sum_{i=1}^{8} \mathcal{C}e^{-\mu R_i}/R_i\right] \tag{13}$$

very well. By doing three-parameter fits with Eq. (13), we

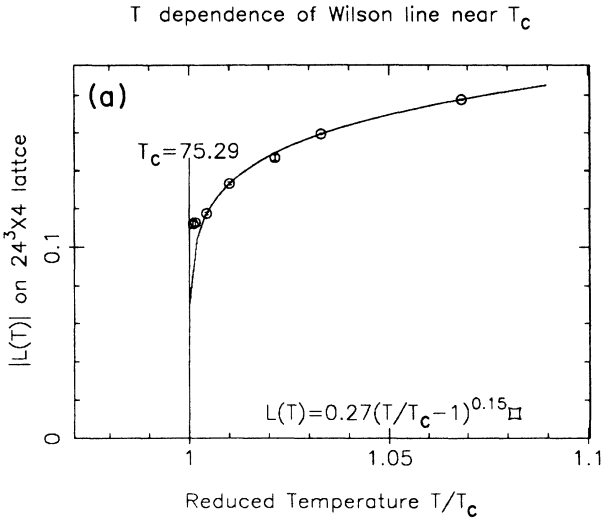

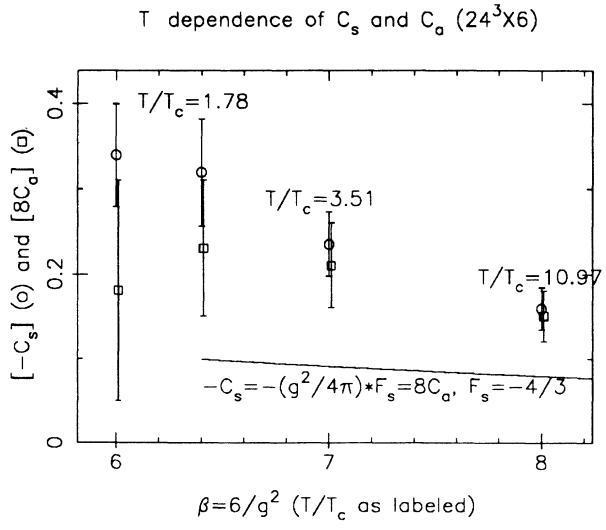

FIG. 6. $\mathcal{C}_s$ and $\mathcal{C}_a$ at various temperatures above T_c but not $\sim T_c^+$. The measurement is done on a $24^3\times 6$ lattice and $\mathcal{C}_s(T)$ and $\mathcal{C}_a(T)$ are defined by Eq. (5).

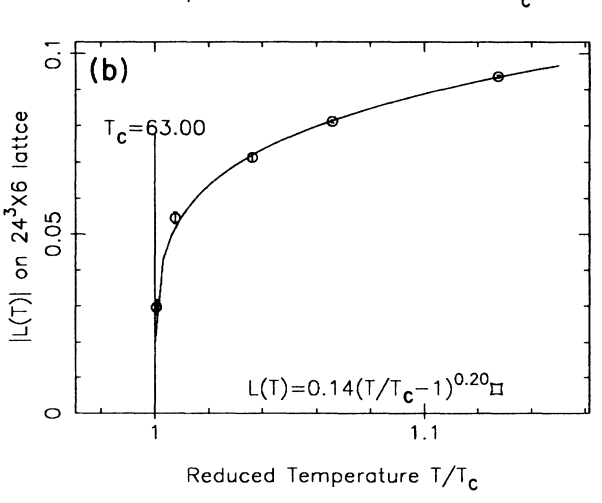

FIG. 7. The critical behavior of the order parameter $|L|$.

can get good measurements on $L(T)$, $\mathcal{C}(T)$, and $\mu(T)$. We will discuss some of them in this subsection. [$\mathcal{C}(T)$ for $N_t=4,6,16$ are shown by Fig. 5 and discussed in IV B.]

The fitted $L(T)$ at various β's agrees well with direct measured $L(T)$ and even has smaller errors. Thus, it is perhaps a better way for measuring the magnitude of the Wilson line than the direct measurement especially near the critical point. $L(T)$ gives us $\mathcal{F}_q$.

The T dependence of $L(T)$ (or $\mathcal{F}_q$) is interesting. For T is quite close to T_c (say, $T_c<T<1.005T_c$), we see the rapid variation of L during the simulation and L has the clear visible discontinuity required by a first-order transition. Phase mixing makes the measurement of L more complicated (no unique way to separate the two phases). However, for $T>1.01T_c$, the phase is well defined with no mixing. $L(T)$ shows some critical scaling behavior for regions of temperature where T is close to T_c but not too close. It fits the scaling function (fractional power)

$$L(T)\sim\exp(-\mathcal{F}_q/T)\sim A(T-T_c)^{\bar{\beta}} \tag{14}$$

very well in this region. Figures 7(a) and 7(b) show results of a three-parameter fit to Eq. (14) for each one of $N_t=4,6$ cases, respectively (fitted parameters are also shown in the figures). Within errors, the fitted fractional powers ($\bar{\beta}$'s) agree with each other. Note that $T/\Lambda_L=62.9\pm0.1$ ($\beta_c=5.892\pm0.002$), and $T/\Lambda_L=75.30\pm0.07$ ($\beta_c=5.6916\pm0.0003$) for $N_t=6,4$, respectively, agree very well with the other fitted T_c from the critical behavior of the string tension.[9] The results are also consistent with our knowledge obtained from the time evolution during the simulation and other measured quantities such as fractional confined, etc. The agreement between the results from different methods is a surprising and interesting result.

The observed scaling behavior adds some interesting features to the deconfinement phase transition. Authors of Ref. 11 have found similar behavior for the three-state Potts model in $d=3$ from a Monte Carlo renormalization group analysis. They concluded that the nature is a "first-order phase transition but almost second order." It is possible that the first-order deconfinement phase transition is superposed by a second-order-like behavior.

D. Correlation length and the phase transition

The asymptotic correlation length near the phase transition point is given by the inverse of the screening mass. The measured Debye screening masses have been shown by Figs. 4 and 5 in Ref. 11 (including the measured string tensions). More discussion on them will be given by a further publication.[12] They show a rapid increase after the phase transition. Since $L(T)$ also shows a rapid increase in the same region (or decrease in $\mathcal{F}_q$), which means that the $q,\bar{q}$ and other color charged entities can be produced more and more easily, the density of screening particles increases significantly as a result. This in turn makes the screening effect stronger and stronger. The observed rapid increase of the screening mass after the phase transition may well be the consequence of it.

One important observation from measured string tensions and screening masses is that the correlation length (which can be defined as the inverse of the screening mass of the inverse of the string tension) is finite during the phase transition. Even though there is an apparent dip in σ and μ (i.e., a peak in correlation length), the maximum correlation length is still only about ~7 (for $N_t=4$). This is clearly much smaller than $N_s/2=12$ (in our case). Thus the correlation length is not bound by the volume and has a real, finite maximum. The finite correlation length at the phase transition is the other important proof that the phase transition is first order [for $N_t=4$ at least (Ref. 11)]. It should be divergent ($\sim N_s/2$ or N_s for a finite-size lattice as would be implied by the finite-size scaling) for a continuous phase transition. This is also an important result from our simulation.

V. CONCLUSION

As we get closer to the critical temperature, the system becomes more and and more nonperturbative and nontrivial. The dynamics of the gauge theory and the behavior of quark potential are poorly understood. Even at extremely high temperature, the perturbative theory for the QCD still suffers from a very serious breakdown problem. It is interesting and important to do a nonperturbative study to get some qualitative results. Our results start to fill the gap.

Our results of WLC show that the hot gluon plasma supports the Debye picture very well. The heavy-quark potential $V_{q\bar{q}}$ for each representation is essentially a Yukawa-type potential. Thus, Eq. (5) is expected to be the right correlation function and the justification for it can be made from our simulation. Equation (5) implys a thermal averaged potential (at large separation) of the form

$$V(T,\mathbf{R})=\mathcal{C}(T)\exp[-m_D(T)|\mathbf{R}|]/|\mathbf{R}|^n, \tag{15}$$

in two interesting regions where $n\sim1$ for $T\sim T_c$ and $n\sim2$ for $T\gg T_c$. A Debye-type screening mass can be well measured based on this potential. The T dependence of the screening mass tends to agree well with the "perturbative results" at high temperature. This is consistent with the asymptotic expectation. But it has a rapid increase associated with the phase transition where density of color charged entities rises rapidly. Since the screening mass seems to be finite when $T=T_c^+$, it may have a discontinuity. The discontinuity of the mass gap might be associated with the breaking of the string due to the strong screening. How it is related to the phase transition is still an open question.

At very high temperature, an effective "single massive gluon exchange" process seems to be the dominant dynamic process since both $\mathcal{C}_s$ and $\mathcal{C}_a$ tend to agree with their lowest-order perturbative predicted behavior. But near T_c, $\mathcal{C}$'s come from multigluon exchange between two quarks or may even come from nontrivial physics process. Also, the distinction between the two $\mathcal{C}$'s disappears, influenced by the confining characters.

Our qualitative results should provide lots of useful information for heavy-ion collisions and other experiments. The screening effect is possibly responsible for the J/ψ

suppression.[13] The heavy-quark spectra can also be calculated from our potential. Further study on physical consequences still needs to be done.

ACKNOWLEDGMENTS

The author thanks Professor N. H. Christ for his encouraging discussions, suggestions, and advice. The author thanks Dr. S. Ohta for many useful discussions, T. J. Woch and N. H. Christ for their help in installing and maintaining the 64-node parallel processor, and P. Hsieh and Y. Deng for their programing assistance. This research was supported in part by the U.S. Department of Energy.

[1]H. Satz, Nucl. Phys. **A418**, 447c (1984); K. Kanaya and H. Satz, Phys. Rev. D **34**, 3193 (1986).

[2]T. A. DeGrand and C. E. DeTar, Phys. Rev. D **34**, 2469 (1986).

[3]N. Attig *et al.*, Phys. Lett. B **209**, 65 (1988); J. Engles *et al.*, Nucl. Phys. **B315**, 419 (1989).

[4]S. Nadkarni, Phys. Rev. D **33**, 3738 (1986); **34**, 3904 (1986).

[5]C. E. DeTar, Phys. Rev. D **32**, 276 (1985); S. Nadkarni, *ibid.* **27**, 917 (1983).

[6]M. S. Gao, in *Lattice Gauge Theory Using Parallel Processors,* edited by X. Y. Li, Z. M. Qiu, and H. C. Ren (Gordon and Breach, New York, 1987), p. 369.

[7]N. H. Christ and A. E. Terrano, IEEE Trans. Comput. **33**, 344 (1984); Byte **11**, 145 (1986).

[8]M. S. Gao, in *Proceedings of the Storrs Meeting,* Annual Meeting of the Division of Particles and Fields of APS, Storrs, Connecticut, 1988, edited by K. Haller *et al.* (World Scientific, Singapore, 1989).

[9]M. S. Gao, in *Lattice '88,* proceedings of the International Symposium, Batavia, Illinois, 1988, edited by A. S. Kronfeld and P. B. Mackenzie [Nucl. Phys. B (Proc. Suppl.) **9** (1989)].

[10]F. R. Brown, N. H. Christ, Y. F. Deng, M. S. Gao, and T. J. Woch, Phys. Rev. Lett. **61**, 2058 (1988).

[11]H. W. J. Blote and R. H. Swendsen, Phys. Rev. Lett. **43**, 799 (1979).

[12]F. R. Brown, N. H. Christ, Y. F. Deng, M. S. Gao, and T. J. Woch (unpublished).

[13]T. Matsui and H. Satz, Phys. Lett. B **178**, 416 (1986).